1

2

Thermocatalytic conversion of lignin in an ethanol/formic acid medium with NiMo catalysts: role of the metal and acid sites

Mikel Oregui-Bengoechea[a], Nemanja Miletić[b], Sveinung F. Simonsen[a], Audun Kronstad[a], Inaki Gandarias[b], Pedro L. Arias[b] and Tanja Barth[a]

[a] *Department of Chemistry, University of Bergen, Norway, Allegaten 41, N-5007 Bergen, Norway*

[b] *Department of Chemical and Environmental Engineering, School of Engineering, University of the Basque Country (EHU/UPV), C/Alameda Urquijo s/n,48013 Bilbao, Spain*

Keywords: lignin, formic acid, NiMo catalyst, alumina, zirconia

Abstract

NiMo catalysts supported on different sulfated and non-sulfated aluminas and zirconias were studied for the catalytic conversion of lignin in a formic acid/ethanol medium. All the pre-reduced NiMo-support combinations resulted in high conversion of lignin into bio-oil, with over 60 % yield (mass %). The NiMo-sulfated alumina catalyst exhibited the highest activity among all the catalyst studied. The overall reaction mechanism of the catalytic lignin conversion was found to be especially complex. The oil yield and its properties are affected by a combination of successive catalytic reactions that are part of the lignin conversion process. Lignin is first de-polymerized into smaller fragments through the cleavage of the aliphatic ether bonds. This reaction can be either catalyzed by Ni^0 species and strong Lewis acid sites within the alumina supports. In the presence of both active species, the Ni^0 catalyzed ether bond cleavage is the prevailing reaction mechanism. In a second step, the smaller lignin fragments can be stabilized by catalytic hydrodeoxygenation (HDO) and alkylation reactions that hinder their re-polymerization into char. Mo was found to be especially active for HDO reactions while all the catalyst studied exhibited significant alkylation activity. The final bio-oil yield is strongly dependent on the aliphatic ether bond cleavage rate; the contribution of those monomer stabilization reactions (i.e. HDO and alkylation) being secondary.

1. Introduction

The use of lignocellulosic biomass as a raw material for the production of renewable fuels and chemicals is growing rapidly. Consequently, there is an increasing interest in the development of integrated models for the efficient valorization of woody biomass (i.e. as lignocellulosic bio-refineries). Over the last decades, most of the effort has been focused on the development of more efficient lignocellulose pretreatment technologies and the subsequent conversion of the cellulose and hemicellulose fraction into bio-ethanol [1-3] and/or value-added chemicals [4]. In contrast, the third component, lignin, is mostly considered a waste and it is normally burned as a low value fuel [5]. However, the expected growth of the production of lignocellulosic-based products will demand the efficient valorization of the lignin sub-product and the conceptual integration of its conversion processes in the so-called bio-refinery concept.

A plausible process that could meet these requirements is the recently developed LtL process [6, 7]. Formic acid, one of the main sub-products from the cellulose and hemicellulose

47 hydrolysis and sugar conversion processes [8, 9], can react together with lignin in an ethanol

48 media to yield a mono-aromatic based oil, with considerable chemical stability and low oxygen

49 content. This process is carried out under severe reduction conditions: formic acid is decomposed

50 mainly into CO_2 and H_2 providing high reaction pressures. Nevertheless, the LtL conversion

51 requires high temperatures, in the range of 300-360 °C, and long residence times for complete

52 lignin conversion. The process severity would imply a high cost at industrial scale, and at present,

53 the oil yields and its quality are not sufficient to produce LtL oils competitive with traditional

54 fossil-based products [10, 11].

55   A possible option in order to decrease the process severity and simultaneously increase

56 the LtL oil yield and quality – i.e. a higher H/C and lower O/C ratio- is the use of heterogeneous

57 catalysts. Recently Zhang and co-workers [12] described the most important catalytic routes for

58 the conversion of lignin in a reductive environment (hydroprocessing), and the most relevant

59 conversion mechanism were: (i) the catalytic hydrogenolysis of the aliphatic ether bonds of the

60 lignin biopolymer and (ii) the catalytic hydrodeoxygenation (HDO) of the lignin monomers. For

61 the catalytic hydrogenolysis of lignin, Ni-based catalysts are normally the preferred choice (e.g.,

62 Raney Ni, Ni/SiO_2, Ni/activated carbon) [13-15]. In the case of HDO, nonetheless, three different

63 types of catalysts have been studied: monometallic, bimetallic and bifunctional. The

64 monometallic catalysts consist mainly of Mo-supported catalysts [12]. The bimetallic systems

65 refer typically to the combination of mixed sulfides of Co, Ni, Mo and W. Nevertheless, sulfided

66 catalysts are not entirely adequate since they increase the amount of sulfur containing compounds

67 in the liquid products [12, 16]. Bifunctional catalysts in turn contain both metal and acid sites

68 [17]. Several combinations of hydrogenating (e.g. Ni Raney, Pd/C, Pt/Al_2O_3) and solid-acid

69 catalysts (e.g. HZSM-5 and $Nafion/SiO_2$) [18-20], or even bifunctional catalysts (e.g. Ru/HZSM-

70 5, Ni/HZSM-5) [21, 22] have been studied, mostly with lignin model compounds as starting

71 materials.

72   However, very little research has been conducted in the catalytic hydroprocessing of a

73 real lignin feedstock [12, 23]; and even less in the formic acid aided lignin conversion [24]. In a

74 previous study, we investigated the role of formic acid and the solvent (i.e. ethanol) in the

75 catalytic lignin conversion with a NiMo supported on a sulfated Al_2O_3, a Lewis solid acid [25].

76 The investigations revealed that the catalytic lignin conversion into bio-oil follows a complex

77 reaction pathway. In the presence of formic acid, lignin undergoes de-polymerization through a

3

78   formylation-deformylation-hydrogenolysis pathway that leads to the cleavage of its aliphatic

79   ether bonds. The depolymerized monomers and oligomers can undergo subsequent

80   hydrodeoxygenation (HDO) and alkylation reactions. These reactions tend to stabilize the lignin

81   monomers hindering their re-polymerization into char (Scheme 1).

82

83   Scheme 1. Sequential reaction scheme for the conversion of lignin into bio-oil. * The term

84   compounds may refer to both monomers and/or oligomers. This is an adapted scheme based on a

85   previous study [25].

86   To further explore these processes, the catalytic role of the type of metal (i.e. Ni and Mo),

87   the Lewis acidity and the metal-support interaction on the lignin de-polymerization (i.e. aliphatic

88   ether bond cleavage) and monomer stabilization reactions (i.e. HDO and alkylation) is studied

89   using well-characterized heterogeneous catalysts. Moreover, the relative importance of each

90   reaction pathway (de-polymerization vs. stabilization) on the oil yield and oil quality is also

91   assessed. For this purpose, several combinations of non-sulfided monometallic (*i.e.* Ni and Mo)

92   and bimetallic NiMo catalysts supported on zirconia and γ-alumina are evaluated. Sulfated

93   zirconia [26, 27] and alumina [28] are also used as catalyst supports to further explore the effect

94   of the Lewis acidity strength in the reaction mechanism. The recyclability of the NiMo catalyst in

95   the LtL conversion process is also examined.

96

2. Experimental

2.1 Chemicals

Formic acid (>98%), tetrahydrofuran (>99.9%), ethyl acetate (99.8%), hexadecane (>99.8%), sulfuric acid (95-97%), anhydrous sodium sulphate (>99.0 %) and zirconium (IV) hydroxide (97%) were purchased from Sigma Aldrich and used as supplied. γ-alumina (>97%), nickel(II) nitrate hexahydrate (99.9+% Ni) and ammonium molybdate tetrahydrate (99.98% Mo) were purchased from Strem Chemicals Inc and used as received. The Technical College of Bergen supplied rice straw lignin from a strong acid carbohydrate dissolution pre-treatment. The lignin was ground and sieved (<500 µm) prior to use. The elemental composition and the inorganic ash content of the rice straw lignin are given in Table S1, *Supplementary Information*.

2.2 Synthesis of the catalyst

2.2.1 Synthesis of the supports

Non-sulfated alumina: γ-alumina was dried at 100 °C for 24 h prior to use. This support is named AL.

Non sulfated zirconia: ZrO_2 was obtained by calcining $Zr(OH)_4$ at 600 °C for 4 h with a heating ramp of 3°C/min. The resulting support is denoted as ZR.

Sulfated alumina: γ-alumina was subjected to a thermal treatment in air at 450 °C for 4 h with a heating ramp of 3 °C/min. The calcined alumina was impregnated (4 cm^3 sulfuric acid/cm^3 of pore) with a sulfuric acid solution (mass fraction of 0.5 %) and stirred for 24 hours. The solution was dried at 80 °C for 24 h and the resulting solid was calcined at 600 °C for 4 h with a heating ramp of 3 °C/min. The resulting sulfated alumina is denoted as SAL.

Sulfated zirconia: $Zr(OH)_4$ was impregnated (5 mL/g) with a sulfuric acid solution (0.5 M) and stirred for 2 h. The solution was dried at 80 °C for 24 h and the resulting solid was calcined at 600 °C for 4 h with a heating ramp of 3 °C/min, obtaining the sulfated zirconia (SZ). This support is denoted as S-ZR.

2.2.2 Synthesis of the metallic catalysts

The bimetallic catalysts were later prepared by successive incipient-wetness impregnation of the corresponding support (AL, SAL, ZR and SZR) with an aqueous solution of ammonium molybdate $(NH_4)_6Mo_7O_{24} \cdot 4H_2O$ and/or nickel nitrate $(Ni(NO_3)_2 \cdot 6H_2O)$. The nominal loading of MoO_3 and NiO are 12 % and 5 % respectively, given as mass fraction percentage. After impregnation, the catalysts were dried at 105 °C for 20 min and calcined in an air flow (10 mL/min) at 570 °C for 2 h with a heating ramp of 2 °C/min. Later, the solids were subjected to pre-reduction (activation) under a hydrogen flow (10% v/v) at 550 °C for 2 h with a heating ramp of 2 °C/min and used shortly after the treatment. The resulting bimetallic catalysts are named H-NiMo-AL, H-NiMo-SAL, H-NiMo-ZR and H-NiMo-SZR. Two monometallic catalysts were synthesized with the SAL support: one containing only Ni (H-Ni-SAL) and the second containing only Mo (H-Mo-SAL). The metal loading and the synthesis procedure were equivalent to the ones used for their bimetallic counterparts.

The bare supports (AL, SAL, ZR and SZR) were analyzed by N_2-adsorption, FT-IR of adsorbed pyridine, NH_3-TPD, and XRD. The bimetallic H-NiMo-AL, H-NiMo-SAL, H-NiMo-ZR, H-NiMo-SZR, H-Ni-SAL and H-Mo-SAL catalysts were analyzed by N_2-adsorption, NH_3-TPD, ICP-EAS, XRD, TPR and CO-chemisorption. The experimental procedures for the characterization of the catalyst are described in the *Supplementary Information*.

2.3 LtL experiments

2.3.1 Experimental set-up

A detailed description is given elsewhere by Oregui Bengoechea *et al.*[10]. Briefly summarized, lignin (2.0 g), formic acid (1.5 g), ethanol (2.5 g) and the catalyst (0.2 g) were added to a stainless steel reactor (Parr 4742 non-stirred reactor, 25 mL volume). The reactor was closed and heated up to 340 °C in a Carbolite LHT for 6 h. Two replicates were performed for each experiment. The results refer to the average values of both experiments. The amounts of the reactants used for all the experiments are summarized in Table S2, *Supplementary Information*.

2.3.2 Work-up procedure

After heating for the predetermined duration, the reactor was cooled down to ambient temperature by natural convection. The liquid mixture within the reactor was extracted with a solution of ethyl acetate:tetrahydrofuran (90:10) and the solid phase (unreacted lignin, reaction products and catalyst) was filtered off. The resulting liquid phase was dried over Na_2SO_4 and concentrated at reduced pressure (160 mm bar) at 40 °C to yield a dark-brown to black liquid. The oil and solid yield are given as mass fraction % and were determined using the following equation:

Oil/Solid Yield (mass fraction %) = dry mass of oil or solids (g)/dry mass of input lignin (g)

For the catalyzed experiments, the solid yield was calculated after subtracting the amount of catalyst introduced. Therefore, the solid yield refers only to the organic solids (char) and the inorganic lignin ashes.

The oil was analyzed by GC-MS and GPC-SEC. Its elemental composition was also determined. The procedures used for the characterization of the oils are described in the Supplementary Information.

2.3.3 Recycling experiments

After the reaction, the solids (organic ashes, inorganic ashes and catalysts) were recovered and calcined at 570 °C for 2h with a heating ramp of 2 °C/min to eliminate the organic residues. The resulting solids (catalyst and inorganic ashes) were pre-reduced at the same conditions described in *Section 2.2.2* and re-used in the LtL process. After the first recycling cycle, a higher amount of solid was recovered due to inorganic ash accumulation in the system. Therefore, to guarantee the proper reduction of the catalyst, in the second recycling cycle the pre-reduction of the catalyst was carried out for 3 h.

Blank experiments were also carried out to evaluate the activity of the inorganic ashes. The experimental procedure is analogous to the one described in *Section 2.3.1*, but in this case, instead of catalysts, 0.2 g of inorganic ashes were added (ASH-1 experiment). The method used to obtain the inorganic lignin ashes is the same used to determine the lignin ash content (*Supplementary Information*).

3. Results

3.1 Catalyst Characterization

3.1.1 N$_2$-adsorption

The textural properties of the catalysts are presented in Table 1 and Fig. 1. The results show that the sulfating process has different effects on the textural properties of the alumina and zirconia supports. In the case of the alumina catalysts, small differences between the sulfated and non-sulfated counterparts are observed: the sulfated solids display slightly higher surface areas. The alumina-based solids (AL, SAL, H-NiMo-AL and H-NiMo-SAL) exhibit an IUPAC Type IV isotherm typical for mesoporous materials. The catalysts (H-NiMo-AL and H-NiMo-SAL) present a lower surface area and V_t than their corresponding bare supports (AL and SAL) suggesting that the incorporation of the Ni and Mo causes the partial blockage of the pores [29].

Table 1: BET surface area (S$_{BET}$), total pore volume (V_t), total acidity measurements (NH$_3$-TPD), NiO and MoO$_3$ content (ICP-EAS) and number of nickel active sites (CO-chemisorption) for the bare supports (AL, SAL, ZR, SZR) and metallic catalyst (H-NiMo-AL, H-NiMo-SAL, H-NiMo-ZR, H-NiMo-SZR, H-Ni-SAL, H-Mo-SAL).

Entry	Catalyst[a]	S$_{BET}$ (m^2/g)	V_t (cm^3/g)	Acidity (mmol NH$_3$/g cat.)		ICP-MS		No. of Ni active sites (µmol CO/g cat)
				Weak	Strong	NiO	MoO$_3$	
				85-340°C	340-590°C	(mass fraction %)		
1	AL	198	0.416	0.420	0.390	-	-	-
2	H-NiMo-AL	172	0.328	0.521	0.366	4.7	11.4	18.5
3	SAL	202	0.414	0.485	0.397	-	-	-
4	H-NiMo-SAL	179	0.335	0.547	0.375	3.6	10.7	6.9
5	H-Ni-SAL	183	0.369	0.374	0.589	5.8	-	12.6
6	H-Mo-SAL	181	0.347	0.467	0.335	-	11.7	-
7	ZR	11	0.032	0.056	0.054	-	-	-
8	H-NiMo-ZR	15	0.010	0.045	0.026	5.2	11.7	2.1
9	SZR	71.2	0.074	0.289	0.126	-	-	-
10	H-NiMo-SZR	42.4	0.066	0.146	0.067	4.6	10.0	0.7

[a] **H** refers to those catalyst that were submitted to a pre-reduction treatment, **NiMo:** bimetallic catalysts containing Ni and Mo, **Ni:** monometallic catalyst containing only Ni, **Mo:** monometallic catalyst containing only Mo, **AL:** γ-alumina, **SAL:** sulfated alumina, **ZR:** zirconia and **SZR:** sulfated zirconia

198   The textural properties of the zirconia support, however, are considerably altered upon

199   sulfating. The non-sulfated zirconia solids (ZR and H-NiMo-ZR) exhibit adsorption-desorption

200   isotherms with a hysteresis loop at high relative pressures (Figure 1c) generally assigned to the

201   presence of mesopores [30]. Nevertheless, the low surface area and V_t found in these solids

202   (*entries 7-8,* Table 1) suggest that this hysteresis is due to nanoparticle-aggregation [31]. Thus,

203   the ZR and H-NiMo-ZR solids are either macro- or non-porous. The sulfated zirconia solids

204   (SZR and H-NiMo-SZR), on the other hand, are mesoporous solids and exhibit considerably

205   higher surface areas than their non-sulfated counterparts. The sulfated zirconia solids (SZR and

206   H-NiMo-SZR) show a IUPAC Type IV isotherms (Figure 1d) with a large increase in the

207   adsorption at higher relative pressures (p/p_0), which can be assigned to the presence of large size

208   mesopores in the samples [32]. The isotherms also exhibit a sharp-step H2-type hysteresis loop,

209   which can be explained by the interconnectivity of pores [33, 34]. The SZR support exhibits

210   considerably higher surface area and V_t in comparison to the H-NiMo-SZR catalyst, suggesting

211   that the pores are partially blocked by the Ni and Mo species.

212

213
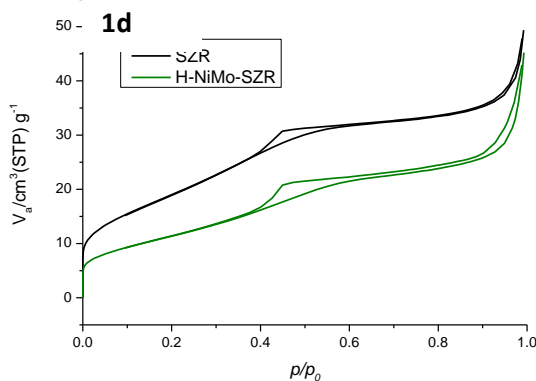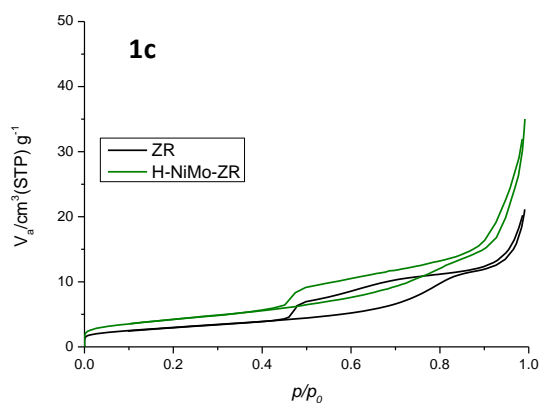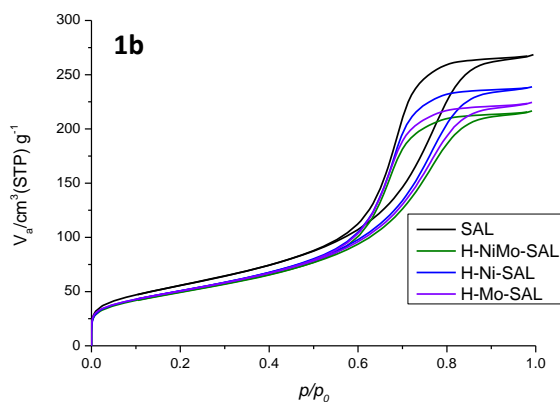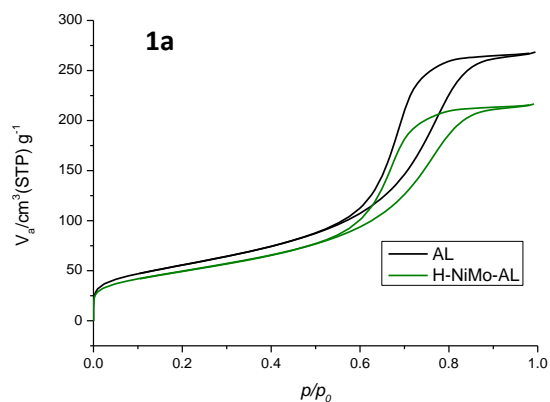
Figure.1 a) N$_2$-adsorption isotherms for the AL (●) and H-NiMo-AL (●) catalysts **b)** N$_2$-adsorption isotherms for the SAL (●), H-NiMo-SAL (●), H-Ni-SAL (●) and H-Mo-SAL (●) catalysts **c)** N$_2$-adsorption isotherms for the ZR and H-NiMo-ZR (●) catalysts **d)** N$_2$-adsorption isotherms for the SZR (●) and H-NiMo-SZR (●) catalysts

3.1.2 Acidity measurements (NH$_3$-TPD and DRIFT of absorbed pyridine)

NH$_3$-TPD and DRIFT of absorbed pyridine are normally combined to determine the strength, concentration and type of acid sites (Lewis or Brønsted) within a solid. The NH$_3$-TPD results are presented in Figure 2 and Table 1, while the DRIFT results are depicted in Figure S1 (*Supplementary Information*). In order to facilitate the analysis, the acid sites are further classified according to their strength. This classification is based on NH$_3$ desorption temperatures. Hence, those acid sites that are not stable below the reaction temperature (<340 °C) were designated as weak, while those acid sites that are stable above the reaction temperature (>340 °C) are designated as strong (Table 1).

227

228
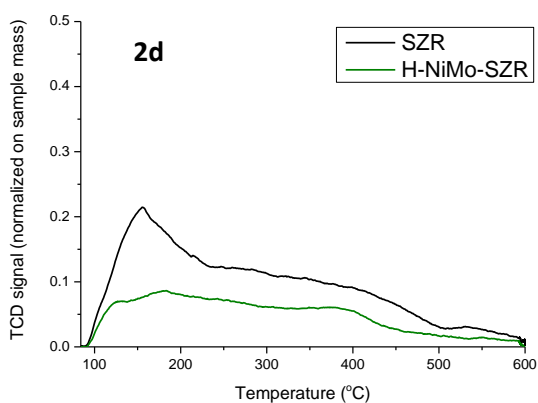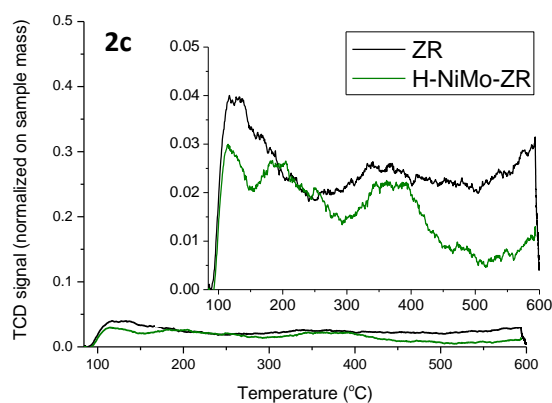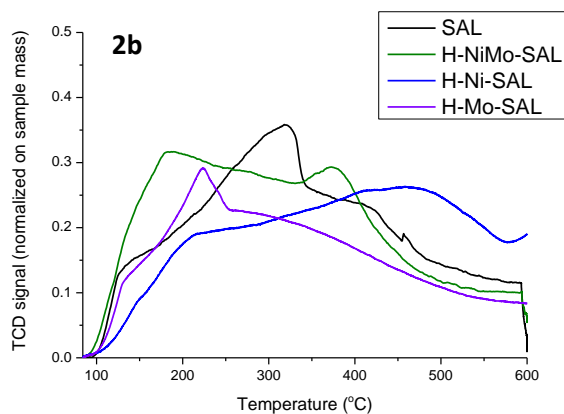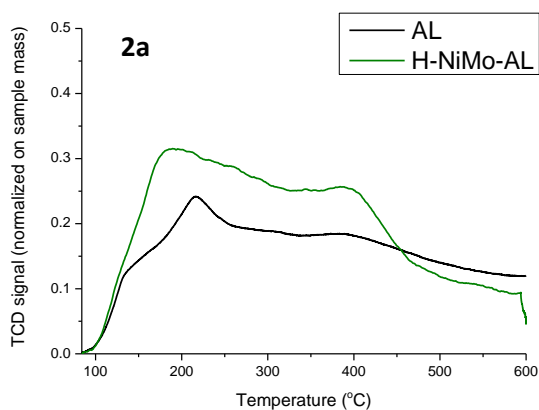
Figure 2a) NH$_3$-TPD for the AL (●) and H-NiMo-AL (●) catalysts **b)** NH$_3$-TPD for the SAL (●), H-NiMo-SAL (●), H-Ni-SAL (●) and H-Mo-SAL (●) catalysts **c)** NH$_3$-TPD for the ZR (●) and H-NiMo-ZR (●) catalysts **d)** NH$_3$-TPD for the SZR (●) and H-NiMo-SZR (●) catalysts

AL, SAL and SZR display acidity in the weak and strong region according to the NH$_3$-TPD results (Figure 2). The ZR support exhibits no significant acidity, nor did its corresponding bimetallic catalysts (H-NiMo-ZR), as observed in Figure 2c and in Table 1 (*entries 7-8*). The DRIFT spectra for the AL, SAL and SZR depicted in Figure S1 indicate that the acidity of these supports is mainly of Lewis nature: the IR bands around 1450 cm^{-1} and 1610 cm^{-1} are associated with pyridine adsorbed on Lewis (L) acid sites. No bands around 1540 cm^{-1} associated with Brønsted (B) acid sites are found for any of the solids [35, 36]. The additional weak IR peak observed around 1495 cm^{-1} is normally attributed to a combination band associated with both B and L sites [36]. Thus, sulfating the alumina did not alter the nature of its acid sites. On the contrary, the zirconia experimented and increase in surface acidity due to the appearance of surface Lewis acid sites.

11

244   The NH$_3$-TPD results presented in Table 1 and Figure 2 also indicate that, in the case of

245   the alumina, the sulfation process did not alter the strength and distribution of the Lewis sites

246   either. Only a slight increase of weak acid sites is observed (0.420 mmol NH$_3$/g cat. for AL and

247   0.485 SAL mmol NH$_3$/g cat.). When compared with their corresponding bare supports, the

248   bimetallic alumina catalyst H-NiMo-AL and H-NiMo-SAL display a larger amount of weak acid

249   sites but a slightly smaller amount of strong acid sites.

250   As mentioned above sulfating the zirconia had a positive effect in the generation of acid

251   sites, significantly increasing the Lewis acidity of the SZR support (Table 1). As depicted in

252   Figure 2d, the majority of the acid sites found in the SZR support are weak. Its corresponding

253   bimetallic catalysts, H-NiMo-SZR, also exhibits substantial acidity although the amount weak

254   and strong acid sites is considerably smaller (Table 1).

255   **3.1.3 ICP-AES**

256   The Ni and Mo loadings shown in Table 1 are given in their oxide form, NiO and MoO$_3$,

257   respectively. The nominal metal loadings are 5.0 % for the NiO and 12.0 % for the MoO$_3$. Two

258   factors seem to affect the Ni content: the sulfation process and the type of support (i.e. alumina or

259   zirconia). Higher amounts of Ni are observed for those catalysts based on zirconia (H-NiMo-ZR

260   and H-NiMo-SZR) and for non-sulfated supports (H-NiMo-AL and H-NiMo-ZR). In the case of

261   the Mo, the sulfation process is the most determinant factor: those non-sulfated supports (H-

262   NiMo-AL and H-NiMo-ZR) give catalysts with higher Mo contents. Thus, the H-NiMo-ZR

263   catalyst has the highest Ni loading followed by the H-NiMo-AL > H-NiMo-SZR >> H-NiMo-

264   SAL. In the case of Mo, the highest loading is obtained for the H-NiMo-ZR followed by the H-

265   NiMo-AL > H-NiMo-SAL > H-NiMo-SZR.

266   **3.1.4 X-ray diffraction (XRD)**

267   The diffractograms depicted for all the alumina catalysts (AL, H-NiMo-AL and SAL,

268   NiMo-SAL and H-NiMo-SAL), are identical (Figure 3a and 3b). The main peaks corresponding

269   to γ-Al$_2$O$_3$ phase are found at 2θ angles of 37.4, 45.9° and 66.7° (Powder Diffraction File (PDF):

270   01-074-2206). On the contrary, the diffractograms of the non-sulfated zirconia catalyst (ZR and

271   H-NiMo-ZR) differ from the sulfated zirconia catalysts (SZR and H-NiMo-SZR) as depicted in

272   Figure 3c and 3d. Both ZR and SZR diffractograms show broad peaks at 30.3°, 35.2°, 50.4° and

12

273　60.2° corresponding to tetragonal ZrO_2 (PDF: 01-088-1007), while the peaks at 24.2°, 28.2°,

274　31.5°, 34.4°, 40,7° and 50.4° are associated to the monoclinic ZrO_2 phase (PDF: 01-088-2390)

275　[37]. The semi-quantitative analysis of the relative abundance of the zirconia phases was carried

276　out based on the reference intensity ratio (RIR) for the most intense monoclinic and tetragonal

277　peaks. The ZR support is about 20 % of tetragonal zirconium oxide and about 80 % monoclinic

278　zirconium oxide, whereas in the SZR support the percentage of tetragonal phase is significantly

279　higher, 70 %. This is in accordance with previous studies [36, 38] claiming that the presence of

280　sulfate retards the conversion of the tetragonal phase to the monoclinic form.
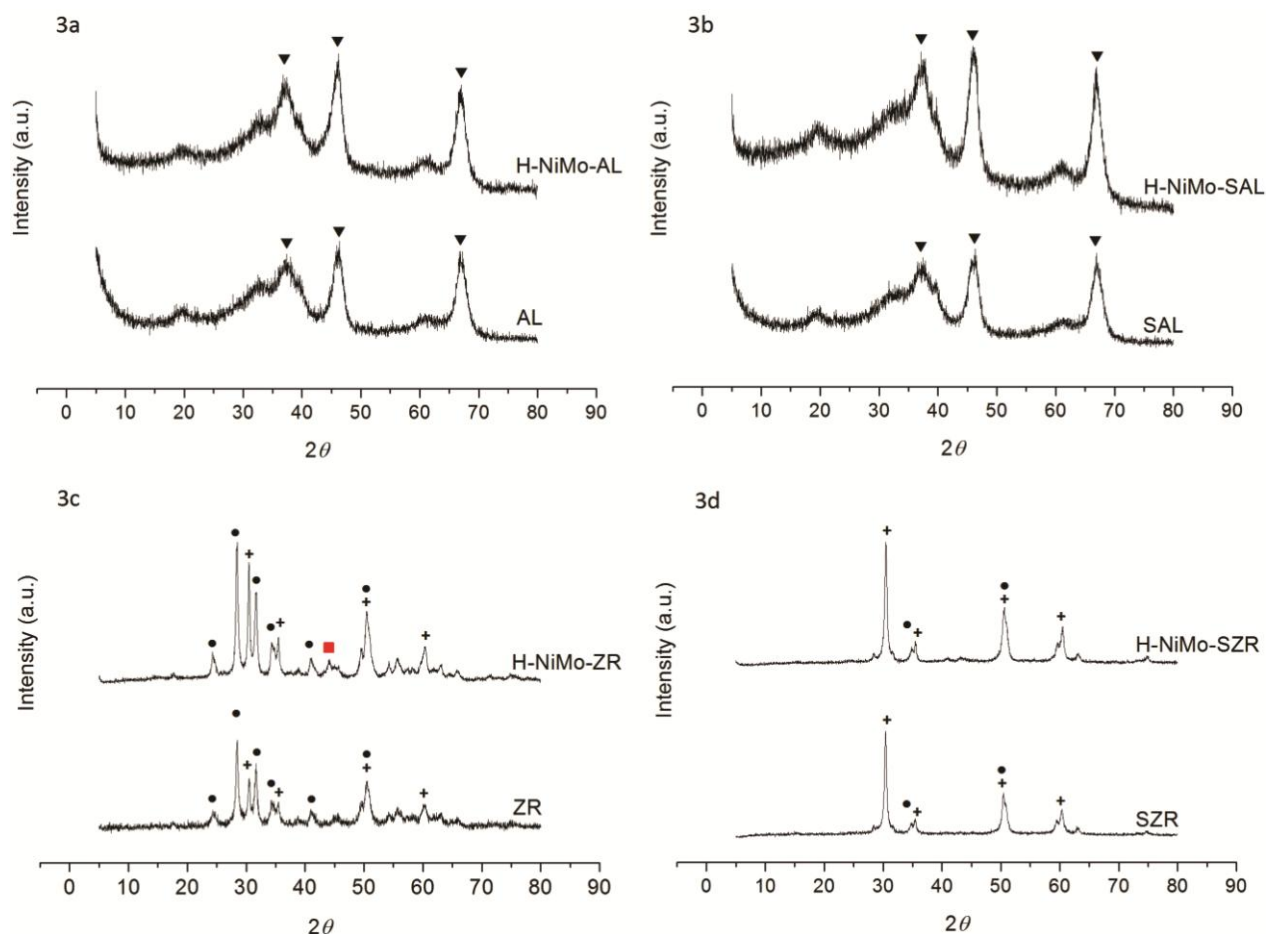
282　**Figure 3a)** XRD difractrograms for the AL and H-NiMo-AL **b)** XRD difractrograms for the SAL and H-
283　NiMo-SAL **c)** XRD difractrograms for the ZR and H-NiMo-ZR and **d)** XRD difractrograms for the SZR
284　and H-NiMo-SZR. (▼) Al_2O_3, (●) monoclinic ZrO_2, (+) tetragonal ZrO_2, (■) Ni.

285

286   Due to the quite low Ni and Mo loadings, identification of chemical phases related to Mo,

287   MoO_x, Ni, NiO or even of $NiMoO_4$ species are not expected. The XRD patterns show no Ni

288   (reflections at 2θ of 44.2°, 51.9°, and 76.1°; PDF: 01-087-0712), NiO (43.6° and 63.2°; PDF#:

289   01-078-0), Mo (40.5° and 73.7°; PDF: 00-042-1120), MoO_3 (27.3°; PDF: 00-001-0706), and

290    $NiMoO_4$ (14.3° and 28.8°; PDF: 00-033-0948) characteristic reflections. Since crystalline

291   particles of sizes below 2-4 nm are undetectable by the XRD technique, most likely these species

292   give rise to very small coherent domains that are homogenously dispersed thought the support

293   matrix or are amorphous. Only, the H-NiMo-ZR catalyst exhibits a characteristic peak for Ni at

294   2θ of 44.2° (Figure 3c).

295   **3.1.5 Temperature-programmed reduction (TPR)**
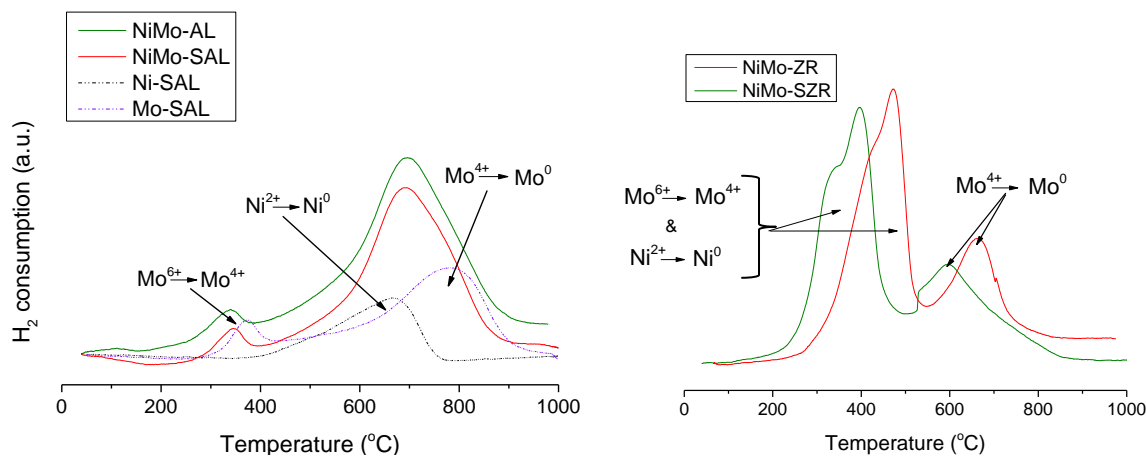
296

297   **Figure 4a)** TPR profile for the NiMo-AL (●), NiMo-SAL (●), Ni-SAL (●) and Mo-SAL (●) catalysts **b)**
298   TPR profile for the NiMo-ZR (●) and NiMo-SZR (●) catalysts

299   Six solids (NiMo-AL, NiMo-SAL, NiMo-ZR, NiMo-SZR , Ni-SAL and Mo-SAL) corresponding

300   to the non-pre-reduced bimetallic and monometallic catalysts (H-NiMo-AL, H-NiMo-SAL, H-

301   NiMo-ZR, H-NiMo-SZR , H-Ni-SAL and H-Mo-SAL, respectively) were characterized by TPR

302   (see Temperature-program-reduction (TPR), *Supplementary Information*). The TPR profiles of

303   the analyzed solids are presented in Figure 4. No significant differences are observed in the shape

304   of the NiMo-AL and NiMo-SAL TPR profiles (Figure 4a). The lower amount of hydrogen

305   consumption observed for the NiMo-SAL can be related to the lower Ni and Mo loading (*Section*

306   *3.1.3*). Thus, sulfating the alumina did not affect significantly the reducibility of the metal

307   species. Both catalysts show two main reduction peaks: a low temperature peak centered around

308   338-344 °C and high temperature broad peak centered at 671-672 °C. The low temperature peak

14

309   corresponds to the partial reduction (Mo^{6+} in Mo^{4+}) of amorphous, highly defective, multilayered

310   Mo oxides or heteropolymolybdates (octahedral Mo species) [39, 40]. The high temperature peak

311   is assigned to a combination of the reduction of Ni^{2+} in Ni^{0} (400-750 °C temperature range) and

312   Mo^{4+} in Mo^{0} (centered around 800 °C), as in can be deduced from the TPR profiles obtained for

313   the monometallic Ni-SAL and Mo-SAL catalysts (Figure 4a).

314   The TPR profiles for the NiMo-ZR and NiMo-SZR (Figure 4b) show that the zirconia

315   support favors the reducibility of the metal species in comparison to the alumina. Both TPR-

316   profiles exhibit comparable shapes. However, the reduction peaks for the NiMo-SZR catalyst are

317   shifted to lower temperatures when compared to the ones for NiMo-ZR, indicating that sulfating

318   the zirconia further decreases the reduction temperature of the Ni and Mo species. The TPR

319   profiles comprise of a complex peak with two maxima and a simple peak, indicating three main

320   reduction processes. According to the literature Ni/ZrO_2 TPRs mainly consist of a reduction

321   temperature peak around 325-475 °C temperature range [41-43]. According to Gutierrez et al.

322   [44] monometallic Mo/ZrO_2 catalysts exhibit two reduction peaks: a lower temperature peak

323   centered around 350 °C corresponding to the reduction of Mo^{6+} to Mo^{4+}, and a high temperature

324   peak centered around 500 °C corresponding to the reduction of Mo^{4+} to Mo^{0}. Thus, the first

325   complex peak corresponds to the reduction of both Mo^{6+} to Mo^{4+} and Ni^{2+} to Ni^{0} while the high

326   temperature reduction peak corresponds to the reduction of Mo^{4+} to Mo^{0}, as previously observed

327   in the literature [45].

328   3.1.6 Chemisorption

329   In this work, the CO-chemisorption technique is employed to determine the number of Ni active

330   sites (given as μmol of CO/g) which is typically related to its catalytic activity (Table 1). The

331   number of Ni active sites is strongly affected by the type of support and sulfation process, the

332   former being the most relevant factor. Alumina supports show a higher dispersion of Ni, so does

333   the non-sulfated supports. Hence, the highest number of active sites is found for the H-NiMo-AL

334   catalyst with $18.5 \cdot 10^{-3}$ mmol CO/g cat. Values comparable in magnitude are observed for the H-

335   NiMo-SAL catalyst with $6.9 \cdot 10^{-3}$ mmol CO/g cat. Conversely, the dispersion and number of Ni

336   active sites for the zirconia catalysts iss poor: $2.1 \cdot 10^{-3}$ mmol CO/g cat for the H-NiMo-ZR and

337    $0.7 \cdot 10^{-3}$ mmol CO/g cat for the H-NiMo-SZR.

3.2 Catalyst effects in LtL conversion

All the experiments were carried out twice. The results shown in Table 2 correspond to the average values of the replicates. When the oil and/or solid yield values differed more than 3.0 percentage points (mass fraction % points), an additional experiment was carried out. Table S3 (*Supplementary Information*) shows the oil and solid yield obtained for the replicates carried out with the bimetallic catalysts (i.e. H-NiMo-AL, H-NiMo-SAL, H-NiMo-ZR and H-NiMo-SZR). No significant differences are observed within the replicates, which confirms that the catalytic LtL experiments are highly reproducible. Note that the content of inorganic ashes of the rice straw lignin used for the LtL experiments is 14.9 % (mass); therefore, the actual organic solid yield, re-polymerized lignin fragments, is considerably smaller than the solid yield shown in the Table 2.

The recovery yield presented in Table 2 indicates the amount of lignin that has been converted into either oil or solid residue. It is also an indirect measurement of the amount of lignin converted to gas and/or the oil and solid that may have been lost during the work-up procedure.

Table 2: Oil, solid and lignin recovery yield, and elemental analysis and M_w of the oils for the catalytic and non-catalytic experiments

| Entry	Experiment[a]	Oil Yield[b]	Solid Yield[b]	Lignin recovery yield[b]	H/C[b]	O/C[b]	M_w[b] (Da)
		(mass %)[c]			molar ratio		
1	NC	36.0	43.5	79.5	1.27	0.13	347
2	AL	50.7	27.0	77.7	1.18	0.14	415
3	SAL	52.0	27.6	79.6	1.17	0.14	382
4	ZR	37.2	32.2	69.4	1.23	0.13	373
5	SZR	41.1	34.8	76.0	1.22	0.14	363
6	H-NiMo-AL	63.7	19.6	83.3	1.22	0.14	410
7	H-NiMo-SAL	64.8	18.7	83.5	1.22	0.14	371
8	H-NiMo-ZR	61.2	20.0	81.2	1.26	0.15	454
9	H-NiMo-SZR	61.9	17.3	79.2	1.25	0.16	421
10	NiMo-SAL	60.2	23.8	84.0	1.22	0.15	387
11	NiMo-SZR	57.5	25.2	82.7	1.26	0.13	355

[a] **NC:** refers to non-catalyzed experiment **H** refers to those catalyst that were submitted to a pre-reduction treatment, **NiMo:** bimetallic catalysts containing Ni and Mo, **Ni:** monometallic catalyst containing only Ni, **Mo:** monometallic catalyst containing only Mo, **AL:** γ-alumina, **SAL:** sulfated alumina, **ZR:** zirconia

and **SZR:** sulfated zirconia [b] Average value of the results obtained in the replicates [c] Relative to the lignin
359 input

3.2.1 Effect of the bare support (AL, SAL, ZR and SZR)

361 The results obtained with the bare supports are compared with the ones obtained for the non-
362 catalyzed (NC) experiment (*entries 1-5,* Table 2). The lignin recovery yields are above a mass
363 fraction of 75 % except for the ZR experiment, meaning that for this experiment a higher amount
364 of oil or solid was either gasified or lost during the work-up procedure.

365 Only the alumina supports (AL and SAL) exhibit catalytic activity towards the de-
366 polymerization of lignin. The highest oil yield, with a mass fraction of 52.0 %, is obtained for the
367 SAL followed closely by the AL support (Figure 5). The oil yield of the zirconia supports (ZR
368 and SZR) is only slightly higher than the non-catalyzed (NC) experiment, confirming their lack
369 of activity.
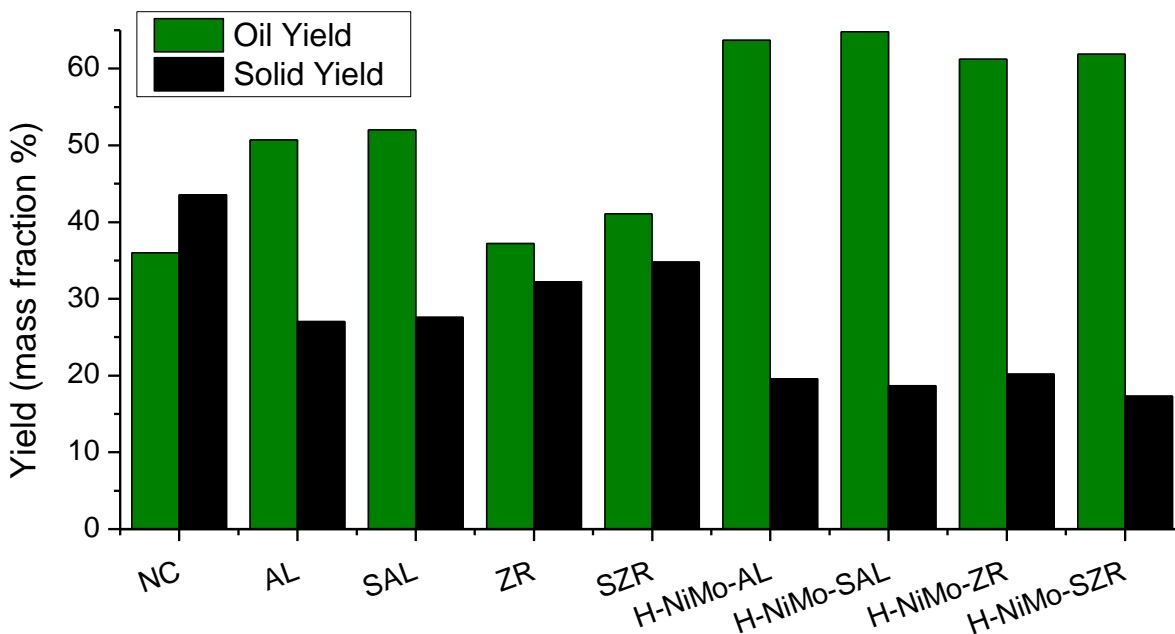
370
371 **Figure 5:** Oil and solid yield for bare supports (NC, AL, SAL, ZR and SZR) and the H-NiMo-AL, H-
372 NiMo-SAL, H-NiMo-ZR and H-NiMo-SZR catalysts. Experiments at 340 °C and 6 h. The oil and solid
373 yield are given in mass fraction %.
374

375   Table S4 (*Supplementary Information*) shows the relative abundance of the main lignin-
376   derived compounds present in the oils. Alkyl substituted phenols are the dominant components.
377   No highly oxygenated compounds, such as substituted guaiacols or catechols, are found; the most
378   oxygenated compounds are ethyl benzoate (EB ether), small amounts of ethoxyphenol (EtPh) and
379   some high molecular weight methoxy- and hydroxy- substituted alkylphenols. Additional intense
380   peaks corresponding to 4-hydroxy-butanoic acid and alkyl esters are also found. It is believed that
381   these compounds are formed due to chemical reactions between formic acid, ethanol and lignin
382   degradation products with the gas components (mainly H_2 and CO_2 produced from the
383   decomposition of formic acid). When comparing the NC oil with those produced in the presence
384   of the bare supports (AL, SAL, ZR and SZR), it is clear that the latter contain a higher amount of
385   highly alkylated single ring phenolics, especially a higher amount of highly alkylated methoxy-
386   and hydroxy-phenols. This suggests that the supports increase the alkylation rate of the
387   monomers. The type of support does not seem to affect significantly the relative amount and type
388   of compounds.

389   **3.2.2 Effect of the bimetallic catalysts (H-NiMo-AL, H-NiMo-SAL, H-NiMo-ZR and H-**
390   **NiMo-SZR)**

391   The bimetallic catalysts (H-NiMo-AL, H-NiMo-SAL, H-NiMo-ZR and H-NiMo-SZR) exhibit
392   higher activities than their corresponding bare supports: Ni and Mo metallic phases significantly
393   increase the oil yields while decreasing the solid yields for all the catalysts studied (*entries 6-9*,
394   Table 2 and Figure 5). The lignin recovery yields also increase to around a mass fraction of 80 %.

395   All the catalysts exhibit similar activities regardless the type of support. The highest oil
396   yield, given as mass fraction %, is obtained for the H-NiMo-SAL (64.8 %), followed closely by
397   the H-NiMo-AL (63.7 %) > H-NiMo-SZR (61.9 %) > H-NiMo-ZR (61.2 %). The solid yields
398   obtained are also significantly lower: all the catalysts give similar solid yields ranging from 17.3
399   % for the H-NiMo-SZR to 20.0 % for the H-NiMo-ZR (Table 2).

400   The bimetallic catalysts yield oils with slightly higher H/C molar ratios than their
401   corresponding bare supports; the O/C molar ratios are comparable or slightly higher (*entries 2-9*,
402   Table 2). The average molecular weight of the oil (M_w) decreases slightly in the case of the
403   alumina-based catalysts (H-NiMo-AL and H-NiMo-SAL), but increases considerably for the
404   zirconia-based ones (H-NiMo-ZR and H-NiMo-SZR). Small differences are also observed in

405   terms of composition of the oils when compared the bimetallic catalyst with the bare supports

406   (Table S4, *Supplementary Information*). The bimetallic catalysts yield oils containing propofol

407   (Prop) and 2-(1,1-dimethylethyl)-3-methylphenol ((dME)MPh); while other compounds such as

408   2,3,5-trimethyl-1,4-benzenediol ((dME)dHB) and 4-(1,1-dimethylethyl)-1,2-benzenediol

409   (dMdMB) are no longer observed. The bimetallic catalysts also produce oils with a larger content

410   of diethyl-phenol (dEPh). Thus, the bimetallic catalyst still yield a higher amount of highly

411   alkylated single ring phenolics when compared with the NC oil.

412   In order to evaluate the effect of pre-reducing (activating) the bimetallic catalyst, two

413   additional experiments were carry out with non-pre-reduced catalysts, i.e. NiMo-SAL and NiMo-

414   SZR (entries 10-11, *Supplementary Information*). These catalysts are the non-pre-reduced

415   counterparts of the most active alumina and zirconia catalysts. The NiMo-SAL and NiMo-SZR

416   catalysts present similar textural (Table S5 and Figure S2) and acidic properties (Table S5 and

417   Figure S3) when compared to their pre-reduced H-NiMo-SAL and H-NiMo-SZR counterparts,

418   although the NiMo-SAL and NiMo-SZR present a larger amount of weak Lewis acid sites. The

419   results presented in Table 2 (*entries 10-11*) show that the oil yields of the non-pre-reduced NiMo-

420   SAL and NiMo-SZR are slightly lower than the ones obtained for their pre-reduced counterparts;

421   the solid yields are slightly higher. For the sulfated alumina catalysts (H-NiMo-SAL and NiMo-

422   SAL), the H/C, O/C and M_w values of the oils are comparable, while in the case of the sulfated

423   zirconia catalysts (H-NiMo-SZR and NiMo-SZR), only the M_w values differ.

424   **3.2.3 Effect of the Ni and Mo**

425   In this section, the activities of monometallic H-Ni-SAL and H-Mo-SAL catalysts are compared

426   with the activity of the bimetallic H-NiMo-SAL catalyst in order to evaluate the role of the Ni

427   and Mo species (Table 3). All the three catalysts are based on the same sulfated alumina support

428   (SAL). The experiments described in this section were performed one year after the ones

429   described in previous sections. Thus, the baseline H-NiMo-SAL experiment was again repeated

430   to take into account the effect of the chemical and physical transformations of lignin upon storage

431   or other serendipity factors. This experiment is labeled R1-NiMo-SAL. The yields are somewhat

432   different, with the oil yield increasing from 64.8 to 76.5 %, but retaining comparable elemental

433   ratios and M_w values.

434

435 **Table 3:** Oil, solid and lignin recovery yield, and elemental analysis and M_w of the oils for the
436 monometallic catalysts and recycled H-Ni-Mo-SAL catalyst.

Experiment[a]	Type of catalyst	Oil Yield[b]	Solid Yield[b]	Lignin recovery yield[b]	H/C[b]	O/C[b]	M_w^b (Da)
		(mass %)			molar ratio		
NC	-	36.0	43.5	79.5	1.27	0.13	347
H-Ni-SAL	Monometallic Ni	72.5	22.4	94.9	1.24	0.15	428
H-Mo-SAL	Monometallic Mo	64.0	31.1	95.1	1.31	0.13	436
ASH	Lignin ashes	42.4	48.5	90.9	1.30	0.13	326
R1-NiMo-SAL	Bimetallic NiMo (fresh, 1st test)	76.5	19.3	95.8	1.22	0.15	397
R2-NiMo-SAL	Bimetallic NiMo (2nd test)	72.7	24.3	97	1.25	0.13	398
R3-NiMo-SAL	Bimetallic NiMo (3rd test)	76.5	21.6	98.1	1.24	0.13	391

437 [a] **NC:** refers to non-catalyzed experiment **ASH:** inorganic ash catalysed experiment, **R1**: experiment with
438 the fresh bimetallic H-NiMo-SAL catalyst, 1st test. **R2:** recycled H-NiMo-SAL bimetallic catalyst 2nd test
439 and **R2**: recycled H-NiMo-SAL bimetallic catalyst 3rd test [a] Average molecular weight of the oil [b] Average
440 value of the results obtained in the replicates [c] Relative to the lignin input

441   The results depicted in Figure 6 and Table 3 show that the bimetallic catalyst (R1-NiMo-

442 SAL experiment) gives the highest oil and lowest solid yields, a mass fraction of 76.5 % and 19.3

443 %, respectively. Still, the oil and solid yields of the monometallic Ni catalyst (H-Ni-SAL) are

444 similar to the ones obtained for the bimetallic R1-NiMo-SAL catalyst, a mass fraction 72.5 % and

445 22.4 %, respectively. The monometallic Mo catalyst (H-Mo-SAL), on the contrary, gives a

446 relatively lower oil yield, mass fraction of 64.0 %, and significantly higher solid yield, mass

447 fraction of 31.1 %. Considerable differences in the properties of the oils are also found (Table 3).

448 The H-Mo-SAL oil has a higher H/C and a lower O/C ratio than the H-Ni-SAL and R1-NiMo-

449 SAL oil; thus, the monometallic H-Mo-SAL catalyst produces a more hydrodeoxygenated oil. In

450 terms of M_w, the lowest values were obtained for the bimetallic R1-NiMo-SA catalyst (397 Da)

451 followed by the monometallic H-Ni-SAL (428 Da) and the H-Mo-SAL (436 Da).
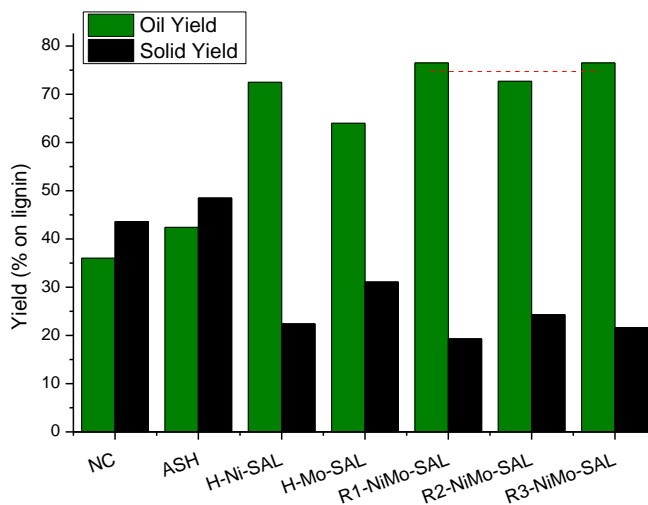
Figure 6 oil and solid yield for the NC, ASH, H-Ni-SAL, H-Mo-SAL, R1-NiMo-SAL, R2-NiMo-SAL and R3-NiMo-SAL experiments

Differences in the oil composition are also found between the monometallic catalysts (Table S6, *Supplementary Information*). In general, the H-Mo-SAL oil has a higher abundance of alkylated phenols such as ethylmethylphenol (EMPh), diethyl phenol (dEPh) and propofol (Prop); while the H-Ni-SAL oil contains methoxy- substituted compounds such as 1-ethoxy-2-methoxy-4-methylbenzene (EtMtMB) and 4-methoxy-2,3,6-trimethyl-phenol (Mt-tMPh), and a larger amount of ethoxyphenol (EtPh). This is in accordance with the elemental analysis and explains the higher H/C and lower O/C ratios obtained for the H-Mo-SAL catalyst.

3.2.4 Recyclability of the H-NiMo-SAL catalyst (R1-NiMo-SAL)

In *Section 3.2.2*, the H-NiMo-SAL was found to be the best catalyst in terms of oil yield and oil properties. Thus, the recyclability of the H-NiMo-SAL catalyst was studied for three consecutive catalytic tests. The experiments are summarized in Table 3 and Figure 6. Note that the R1-NiMo-SAL experiment corresponds to the experiment carried out with the fresh H-NiMo-SAL catalyst as described in the previous section. The R2-NiMo-SAL and R3-NiMo-SAL experiments correspond the second and third test, respectively.

The catalyst was recycled together with the inorganic lignin ashes. Hence, the possible catalytic effect of the inorganic ashes is first evaluated (ASH) in order to subtract this effect from the results obtained upon recycling. The composition of the ashes had been also determined by ICP-MS to connect their possible activity to specific metal species (Table S7, *Supplementary*

473 *Information*). The ASH experiment gives not only slightly higher oil but also higher solid yield

474 than the NC counterpart (Table 3) does. Thus, the ashes seemed to reduce the amount of oil and

475 solid lost during the work-up procedure. There was also an increase in the H/C ratio and a slight

476 decrease in the M_w value of the oil. This could be assigned to the presence of either Fe or Si

477 inorganic species, since the rest of the elements found were in negligible concentrations.

478 However, as observed in Table 3 the activity of the inorganic lignin ashes was insignificant in

479 comparison to the bimetallic H-NiMo-SAL catalyst.

480 All the recyclability tests (Table 3) give similar lignin recovery yields, ranging from a

481 mass fraction of 95.8 % for the R1-NiMo-SAL experiment to 98.1 % for the R3-NiMo-SAL.

482 Regarding the oil yield, no significant decrease after three consecutive tests is observed. A slight

483 oil decrease is detected after the first test (from a mass fraction of 76.5 % for the R1-NiMo-SAL

484 to 72.7 % for the R2-NiMo-SAL), but the oil yield increases again in the third test up to a mass

485 fraction of 76.5 %. The opposite trend is observed for the solid yield: after the first test, the solid

486 yield increases from a mass fraction of 19.3 % for the R1-NiMo-SAL to 24.3 % for the R2-

487 NiMo-SAL, but decreases to 21.6 % for the R3-NiMo-SAL. In terms of elemental analysis, the

488 H/C ratio increases after each test (from 1.22 to 1.24 and 1.25) and the O/C ratio decreases (from

489 0.15 to 0.13) which could be assigned to the effect of the inorganic ashes. The M_w value does not

490 vary.

491 **4. Discussion**

492 As it has been described in the introduction, the conversion of lignin in a formic acid/ethanol

493 medium follows the general reaction pathway depicted in Scheme 1 [25]. Comparable sequential

494 reaction schemes have already been reported for the conversion of lignin in reductive

495 environments [46-51]. Initially, lignin is fragmented into smaller lignin species, both mono- and

496 oligomers, through the cleavage of its aliphatic ether bonds (i.e. de-polymerization). These lignin

497 fragments (oligomers) can further undergo de-polymerization, HDO and alkylation reactions,

498 and/or re-polymerization into char. The hydrodeoxygenated and alkylated lignin fragments

499 exhibit higher chemical stabilities and show lower tendency towards re-polymerization [47, 48,

500 51]. Particularly, in a formic acid/ethanol medium, the aliphatic ether bond cleavage (de-

501 polymerization) is believed to occur through a formylation-deformylation-hydrogenolysis

502 mechanism, where the hydrogenolysis step is catalyzed by a metallic active site [25].

503   Interestingly, the results presented in *Section 3.2.1* prove that the aliphatic ether bond

504   cleavage, *i.e.* lignin de-polymerization, can be catalyzed in the absence of metallic species. Both

505   of the bare alumina supports (AL and SAL) increased the oil and decreased the solid yield

506   indicating that larger amounts of lignin fragments were produced. The results presented in

507   *Section 3.2.1* also prove that less acidic SZR and the non-acidic ZR exhibited no significant

508   activity. This indicates that only strong Lewis acid sites are able to catalyze the de-

509   polymerization of lignin. Both AL and SAL support exhibited high concentration of strong Lewis

510   acid sites, while the less acidic SZR support contained mainly weak Lewis acid sites.

511   Nevertheless, the activity of the strong Lewis acid sites in the aliphatic ether bond

512   cleavage seems irrelevant when compared to the activity of the metallic species: substantially

513   higher oil and lower solid yields are obtained with the bimetallic catalyst in comparison to the

514   bare supports. The relevance of the metal catalyzed mechanism is particularly evident when

515   comparing the zirconia and alumina catalysts: the ZR and SZR bare supports exhibit no catalytic

516   activity when compared to the AL and SAL; however, the bimetallic H-NiMo-ZR and H-NiMo-

517   SZR catalysts exhibit activities comparable to the bimetallic alumina catalysts (H-NiMo-AL and

518   H-NiMo-SAL). The dominance of the metal catalyzed aliphatic ether bond cleavage over the acid

519   catalyzed aliphatic ether bond cleavage has already been reported in hydrogen/water media [52].

520   The elemental analysis, GPC-SEC and GC-MS analysis of the oils also point towards this

521   conclusion. Despite exhibiting different surface acidities, all the bimetallic catalysts produce oils

522   with comparable H/C, O/C and M_w values and oil compositions (Section 3.2.2). Thus, the metal

523   catalyzed aliphatic ether bond cleavage seems to be the dominant reaction mechanism, regardless

524   the type of support. The elemental analysis also indicates that the presence of metallic species

525   have an effect on the properties of the oils, increasing their H/C ratio. The GC-MS analysis of the

526   oils support the proposition that the bare supports and their corresponding bimetallic catalysts are

527   able to increase the abundance of alkylated compounds. Catalytic alkylation could also contribute

528   to the oil yield increase through the stabilization of the lignin monomers [47], although this

529   contribution is believed to be secondary [51].

530

531   To evaluate the distinctive role of the Ni and Mo metallic species in the LtL conversion

532 mechanism additional experiments with monometallic H-Ni-SAL and H-Mo-SAL catalyst were

533 carried out. The results in Section 3.2.3 show that the oil and solid yields obtained for the

534 monometallic Ni catalysts (H-Ni-SAL) are comparable to the ones obtained for the bimetallic

535 NiMo catalyst (R1-NiMo-SAL/H-NiMo-SAL); the monometallic Mo catalysts (H-Mo-SAL),

536 however, gives significantly lower oil and higher solid yields. All this suggests that the Ni species

537 are more active towards aliphatic ether bond cleavage than Mo species (Scheme 1). Conversely,

538 the monometallic Mo catalysts is more active towards HDO of the lignin fragments in

539 comparison to the monometallic Ni catalyst: the H-Mo-SAL catalyst yielded oil with higher H/C

540 and lower O/C ratios and a lower number of oxygenated aromatics when compared with the H-

541 Ni-SAL. This is in accordance with previous studies with lignin model compounds: Ni^0 is known

542 to catalyze the cleavage of aryl ether bonds, while MoO_3 is known to cleavage preferentially

543 phenolic C-O bonds over weaker aliphatic ether bonds [12, 53, 54].

544   Non-pre-reduced NiMo-SAL and NiMo-SZR catalysts exhibit similar activities when

545 compared to their pre-reduced H-NiMo-SAL and H-NiMo-SZR counterparts (Section 3.2.2),

546 which indicates that the LtL environment is able to produce Ni^0 species *in situ*. In order to prove

547 this hypothesis, two non-pre-reduced catalysts, monometallic Ni-SAL and bimetallic NiMo-SAL,

548 were submitted to the LtL environment in the absence of lignin. These catalysts are named Ni-

549 SAL-Used and NiMo-SAL-Used, and their TPR profiles were compared with fresh Ni-SAL and

550 NiMo-SAL (Figure S4). The TPR results confirm that the LtL environment is able to reduce Ni^{2+}

551 to Ni (0). The hydrogen consumption for the fresh Ni-SAL catalyst was 1.061 mmol of H_2/g

552 catalysts, while only 0.5715 mmol of H_2/g catalysts for the used Ni-SAL (*see* TPR analysis,

553 Supplementary Information). A lower H_2 consumption is also observed in the case of the

554 bimetallic catalysts: the hydrogen consumption of the fresh NiMo-SAL is 2.262 mmol of H_2/g

555 catalysts, while in the case of the used NiMo-SAL the hydrogen consumption is 1.306 mmol of

556 H_2/g catalysts.

557   The BET (see Section 3.1.1) and CO-chemisorption (see Section 3.1.6) analysis indicate,

558 however, that not all the Ni species participate to the same extent in the catalytic aliphatic ether

559 bond cleavage. The bimetallic alumina catalysts (H-NiMo-AL and H-NiMo-SAL) exhibit a

560 considerably higher porosity and number of Ni active sites as compared to the bimetallic zirconia

561 catalysts (H-NiMo-ZR and H-NiMo-SZR). Furthermore, the low porosity of the bimetallic

24

562   zirconia catalysts indicates that in the H-NiMo-ZR and H-NiMo-SZR most of the Ni species are

563   found over the outer surface of the supports. Given the comparable oil and solid yield obtained

564   for all the bimetallic catalysts, it is believed that the aliphatic ether bond hydrogenolysis is mainly

565   catalyzed by the outer Ni^0 species. Only the Ni^0 species of the outer surface of the catalyst could

566   interact with the high molecular weight and voluminous lignin fragments. Those Ni species

567   within the pores, on the contrary, could only interact with the smaller lignin monomers.

568   When studying the recyclability of the H-NiMo-SAL catalyst, no deactivation is observed

569   after three consecutive tests. The inorganic ashes do not display a significant catalytic activity in

570   terms of oil and solid yield although they do have an effect on the H/C and O/C ratios.

5. Conclusion

572   The role of Ni, Mo and the acid sites on the overall reaction mechanism of the catalytic LtL

573   conversion in formic acid/ethanol media have been studied. The oil yield and its properties are

574   the product of a combination of successive catalytic reactions. Initially, lignin is de-polymerized

575   into smaller fragments through the cleavage of the aliphatic ether bonds. These fragments can

576   further undergo HDO and alkylation reactions which hinders their repolymerization into char.

577   The results suggest that the catalytic aliphatic ether bond cleavage contributes to a larger extend

578   than catalytic HDO and alkylation reactions to the production of bio-oil. The contribution of the

579   HDO and alkylation reactions is secondary in the case of the oil yield, but do have an effect on

580   the oil properties and compositions.

581   In the absence of metallic species strong Lewis acid sites are able to catalyze the initial

582   aliphatic ether bond cleavage. In the presence of metals (i.e. Ni and Mo), in contrast, the metal

583   catalyzed aliphatic ether bond cleavage mechanism prevails over the acid catalyzed mechanism.

584   Ni^0, particularly those metallic Ni active sites found in the outer surface of the catalyst, are found

585   to be more active than Mo species in the catalytic ether bond cleavage. In contrast, Mo was found

586   to be more active for HDO reactions. All the bimetallic catalysts also exhibited significant

587   activity towards catalytic alkylation.

588

7. References

[1] Y. Zheng, C. Yu, Y.-S. Cheng, C. Lee, C.W. Simmons, T.M. Dooley, R. Zhang, B.M. Jenkins, J.S. VanderGheynst, Integrating sugar beet pulp storage, hydrolysis and fermentation for fuel ethanol production, Applied Energy, 93 (2012) 168-175.
[2] S. Tian, J. Zhu, X. Yang, Evaluation of an adapted inhibitor-tolerant yeast strain for ethanol production from combined hydrolysate of softwood, Applied Energy, 88 (2011) 1792-1796.
[3] S.I. Mussatto, E.M.S. Machado, L.M. Carneiro, J.A. Teixeira, Sugars metabolism and ethanol production by different yeast strains from coffee industry wastes hydrolysates, Applied Energy, 92 (2012) 763-768.
[4] R. Sahu, P.L. Dhepe, A One-Pot Method for the Selective Conversion of Hemicellulose from Crop Waste into C5 Sugars and Furfural by Using Solid Acid Catalysts, ChemSusChem, 5 (2012) 751-761.
[5] R.J.A. Gosselink, E. de Jong, B. Guran, A. Abächerli, Co-ordination network for lignin—standardisation, production and applications adapted to market requirements (EUROLIGNIN), Industrial Crops and Products, 20 (2004) 121-129.
[6] M. Kleinert, T. Barth, Phenols from Lignin, Chemical Engineering & Technology, 31 (2008) 736-745.
[7] M. Kleinert, J.R. Gasson, T. Barth, Optimizing solvolysis conditions for integrated depolymerisation and hydrodeoxygenation of lignin to produce liquid biofuel, Journal of Analytical and Applied Pyrolysis, 85 (2009) 108-117.
[8] L.J. Jönsson, B. Alriksson, N.-O. Nilvebrant, Bioconversion of lignocellulose: inhibitors and detoxification, Biotechnology for Biofuels, 6 (2013) 1-10.
[9] D.J. Hayes, S. Fitzpatrick, M.H.B. Hayes, J.R.H. Ross, The Biofine Process – Production of Levulinic Acid, Furfural, and Formic Acid from Lignocellulosic Feedstocks, Biorefineries-Industrial Processes and Products, Wiley-VCH Verlag GmbH2005, pp. 139-164.
[10] M. Oregui Bengoechea, A. Hertzberg, N. Miletić, P.L. Arias, T. Barth, Simultaneous catalytic de-polymerization and hydrodeoxygenation of lignin in water/formic acid media with Rh/Al2O3, Ru/Al2O3 and Pd/Al2O3 as bifunctional catalysts, Journal of Analytical and Applied Pyrolysis, 113 (2015) 713-722.
[11] L. Liguori, T. Barth, Palladium-Nafion SAC-13 catalysed depolymerisation of lignin to phenols in formic acid and water, Journal of Analytical and Applied Pyrolysis, 92 (2011) 477-484.
[12] C. Li, X. Zhao, A. Wang, G.W. Huber, T. Zhang, Catalytic Transformation of Lignin for the Production of Chemicals and Fuels, Chemical Reviews, 115 (2015) 11559-11624.
[13] Q. Song, F. Wang, J. Xu, Hydrogenolysis of lignosulfonate into phenols over heterogeneous nickel catalysts, Chemical Communications, 48 (2012) 7019-7021.

629 [14] C. Li, M. Zheng, A. Wang, T. Zhang, One-pot catalytic hydrocracking of raw woody biomass into
630 chemicals over supported carbide catalysts: simultaneous conversion of cellulose, hemicellulose and
631 lignin, Energy & Environmental Science, 5 (2012) 6383-6390.
632 [15] X. Wang, R. Rinaldi, Corrigendum: Solvent Effects on the Hydrogenolysis of Diphenyl Ether with
633 Raney Nickel and their Implications for the Conversion of Lignin, ChemSusChem, 5 (2012) 1335-1335.
634 [16] V.N. Bui, D. Laurenti, P. Afanasiev, C. Geantet, Hydrodeoxygenation of guaiacol with CoMo catalysts.
635 Part I: Promoting effect of cobalt on HDO selectivity and activity, Applied Catalysis B: Environmental, 101
636 (2011) 239-245.
637 [17] C. Zhao, J. He, A.A. Lemonidou, X. Li, J.A. Lercher, Aqueous-phase hydrodeoxygenation of bio-
638 derived phenols to cycloalkanes, Journal of Catalysis, 280 (2011) 8-16.
639 [18] C. Zhao, J.A. Lercher, Selective Hydrodeoxygenation of Lignin-Derived Phenolic Monomers and
640 Dimers to Cycloalkanes on Pd/C and HZSM-5 Catalysts, ChemCatChem, 4 (2012) 64-68.
641 [19] C. Zhao, Y. Kou, A.A. Lemonidou, X. Li, J.A. Lercher, Hydrodeoxygenation of bio-derived phenols to
642 hydrocarbons using RANEY[registered sign] Ni and Nafion/SiO2 catalysts, Chemical Communications, 46
643 (2010) 412-414.
644 [20] D.D. Laskar, M.P. Tucker, X. Chen, G.L. Helms, B. Yang, Noble-metal catalyzed hydrodeoxygenation
645 of biomass-derived lignin to aromatic hydrocarbons, Green Chemistry, 16 (2014) 897-910.
646 [21] W. Zhang, J. Chen, R. Liu, S. Wang, L. Chen, K. Li, Hydrodeoxygenation of Lignin-Derived Phenolic
647 Monomers and Dimers to Alkane Fuels over Bifunctional Zeolite-Supported Metal Catalysts, ACS
648 Sustainable Chemistry & Engineering, 2 (2014) 683-691.
649 [22] S.K. Singh, J.D. Ekhe, Towards effective lignin conversion: HZSM-5 catalyzed one-pot solvolytic
650 depolymerization/hydrodeoxygenation of lignin into value added compounds, RSC Advances, 4 (2014)
651 27971-27978.
652 [23] X. Wang, R. Rinaldi, Bifunctional Ni catalysts for the one-pot conversion of Organosolv lignin into
653 cycloalkanes, Catalysis Today, 269 (2016) 48-55.
654 [24] A. Kloekhorst, Y. Shen, Y. Yie, M. Fang, H.J. Heeres, Catalytic hydrodeoxygenation and hydrocracking
655 of Alcell® lignin in alcohol/formic acid mixtures using a Ru/C catalyst, Biomass and Bioenergy, 80 (2015)
656 147-161.
657 [25] M. Oregui-Bengoechea, I. Gandarias, P.L. Arias, T. Barth, Unraveling the Role of Formic Acid and the
658 Type of Solvent in the Catalytic Conversion of Lignin: A Holistic Approach, ChemSusChem, (2017) n/a-n/a.
659 [26] F. Babou, G. Coudurier, J.C. Vedrine, Acidic Properties of Sulfated Zirconia: An Infrared Spectroscopic
660 Study, Journal of Catalysis, 152 (1995) 341-349.
661 [27] E. Zhao, Y. Isaev, A. Sklyarov, J.J. Fripiat, Acid centers in sulfated, phosphated and/or aluminated
662 zirconias, Catalysis Letters, 60 (1999) 173-181.
663 [28] M.L. Guzmán-Castillo, E. López-Salinas, J.J. Fripiat, J. Sánchez-Valente, F. Hernández-Beltrán, A.
664 Rodríguez-Hernández, J. Navarrete-Bolaños, Active sulfated alumina catalysts obtained by hydrothermal
665 treatment, Journal of Catalysis, 220 (2003) 317-325.
666 [29] P. Priecel, L. Čapek, D. Kubička, F. Homola, P. Ryšánek, M. Pouzar, The role of alumina support in the
667 deoxygenation of rapeseed oil over NiMo–alumina catalysts, Catalysis Today, 176 (2011) 409-412.
668 [30] G. Duan, C. Zhang, A. Li, X. Yang, L. Lu, X. Wang, Preparation and Characterization of Mesoporous
669 Zirconia Made by Using a Poly (methyl methacrylate) Template, Nanoscale Research Letters, 3 (2008)
670 118-122.
671 [31] Y. Sun, S. Ma, Y. Du, L. Yuan, S. Wang, J. Yang, F. Deng, F.-S. Xiao, Solvent-Free Preparation of
672 Nanosized Sulfated Zirconia with Brønsted Acidic Sites from a Simple Calcination, The Journal of Physical
673 Chemistry B, 109 (2005) 2567-2572.
674 [32] M.K. Mishra, B. Tyagi, R.V. Jasra, Synthesis and characterization of nano-crystalline sulfated zirconia
675 by sol–gel method, Journal of Molecular Catalysis A: Chemical, 223 (2004) 61-65.

676   [33] J.W. McBain, An Explanation of Hysteresis in the Hydration and Dehydration of Gels, Journal of the
677   American Chemical Society, 57 (1935) 699-700.
678   [34] G. Mason, The effect of pore space connectivity on the hysteresis of capillary condensation in
679   adsorption—desorption isotherms, Journal of Colloid and Interface Science, 88 (1982) 36-46.
680   [35] T.-s. Yang, T.-h. Chang, C.-t. Yeh, Acidities of sulfate species formed on a superacid of sulfated
681   alumina, Journal of Molecular Catalysis A: Chemical, 115 (1997) 339-346.
682   [36] W.-H. Chen, H.-H. Ko, A. Sakthivel, S.-J. Huang, S.-H. Liu, A.-Y. Lo, T.-C. Tsai, S.-B. Liu, A solid-state
683   NMR, FT-IR and TPD study on acid properties of sulfated and metal-promoted zirconia: Influence of
684   promoter and sulfation treatment, Catalysis Today, 116 (2006) 111-120.
685   [37] G. Shi, F. Yu, Y. Wang, D. Pan, H. Wang, R. Li, A novel one-pot synthesis of tetragonal sulfated
686   zirconia catalyst with high activity for biodiesel production from the transesterification of soybean oil,
687   Renewable Energy, 92 (2016) 22-29.
688   [38] A. Corma, Inorganic Solid Acids and Their Use in Acid-Catalyzed Hydrocarbon Reactions, Chemical
689   Reviews, 95 (1995) 559-614.
690   [39] L. Qu, W. Zhang, P.J. Kooyman, R. Prins, MAS NMR, TPR, and TEM studies of the interaction of NiMo
691   with alumina and silica–alumina supports, Journal of Catalysis, 215 (2003) 7-13.
692   [40] M. Henker, K.-P. Wendlandt, J. Valyon, P. Bornmann, Structure of MoO3/Al2O3-SiO2 catalysts,
693   Applied Catalysis, 69 (1991) 205-220.
694   [41] Á. Calafat, N. Sánchez, Production of carbon nanotubes through combination of catalyst reduction
695   and methane decomposition over Fe–Ni/ZrO2 catalysts prepared by the citrate method, Applied
696   Catalysis A: General, 528 (2016) 14-23.
697   [42] J. Ren, X. Qin, J.-Z. Yang, Z.-F. Qin, H.-L. Guo, J.-Y. Lin, Z. Li, Methanation of carbon dioxide over Ni–
698   M/ZrO2 (M = Fe, Co, Cu) catalysts: Effect of addition of a second metal, Fuel Processing Technology, 137
699   (2015) 204-211.
700   [43] Z. Li, X. Hu, L. Zhang, S. Liu, G. Lu, Steam reforming of acetic acid over Ni/ZrO2 catalysts: Effects of
701   nickel loading and particle size on product distribution and coke formation, Applied Catalysis A: General,
702   417–418 (2012) 281-289.
703   [44] O.Y. Gutiérrez, T. Klimova, Effect of the support on the high activity of the (Ni)Mo/ZrO2–SBA-15
704   catalyst in the simultaneous hydrodesulfurization of DBT and 4,6-DMDBT, Journal of Catalysis, 281 (2011)
705   50-62.
706   [45] Y. Duan, Y. Wu, Q. Zhang, R. Ding, Y. Chen, J. Liu, M. Yang, Towards conversion of octanoic acid to
707   liquid hydrocarbon via hydrodeoxygenation over Mo promoter nickel-based catalyst, Journal of
708   Molecular Catalysis A: Chemical, 398 (2015) 72-78.
709   [46] Q. Song, F. Wang, J. Cai, Y. Wang, J. Zhang, W. Yu, J. Xu, Lignin depolymerization (LDP) in alcohol
710   over nickel-based catalysts via a fragmentation-hydrogenolysis process, Energy & Environmental Science,
711   6 (2013) 994-1007.
712   [47] J.R. Gasson, D. Forchheim, T. Sutter, U. Hornung, A. Kruse, T. Barth, Modeling the Lignin Degradation
713   Kinetics in an Ethanol/Formic Acid Solvolysis Approach. Part 1. Kinetic Model Development, Industrial &
714   Engineering Chemistry Research, 51 (2012) 10595-10606.
715   [48] D. Forchheim, J.R. Gasson, U. Hornung, A. Kruse, T. Barth, Modeling the Lignin Degradation Kinetics
716   in a Ethanol/Formic Acid Solvolysis Approach. Part 2. Validation and Transfer to Variable Conditions,
717   Industrial & Engineering Chemistry Research, 51 (2012) 15053-15063.
718   [49] D. Forchheim, U. Hornung, A. Kruse, T. Sutter, Kinetic Modelling of Hydrothermal Lignin
719   Depolymerisation, Waste and Biomass Valorization, 5 (2014) 985-994.
720   [50] A. Kloekhorst, H.J. Heeres, Catalytic Hydrotreatment of Alcell Lignin Using Supported Ru, Pd, and Cu
721   Catalysts, ACS Sustainable Chemistry & Engineering, 3 (2015) 1905-1914.
722   [51] X. Huang, T.I. Korányi, M.D. Boot, E.J.M. Hensen, Catalytic Depolymerization of Lignin in Supercritical
723   Ethanol, ChemSusChem, 7 (2014) 2276-2288.

724   [52] J. He, L. Lu, C. Zhao, D. Mei, J.A. Lercher, Mechanisms of catalytic cleavage of benzyl phenyl ether in
725   aqueous and apolar phases, Journal of Catalysis, 311 (2014) 41-51.
726   [53] T. Prasomsri, M. Shetty, K. Murugappan, Y. Roman-Leshkov, Insights into the catalytic activity and
727   surface modification of MoO3 during the hydrodeoxygenation of lignin-derived model compounds into
728   aromatic hydrocarbons under low hydrogen pressures, Energy & Environmental Science, 7 (2014) 2660-
729   2669.
730   [54] Q. Bu, H. Lei, A.H. Zacher, L. Wang, S. Ren, J. Liang, Y. Wei, Y. Liu, J. Tang, Q. Zhang, R. Ruan, A review
731   of catalytic hydrodeoxygenation of lignin-derived phenols from biomass pyrolysis, Bioresource
732   Technology, 124 (2012) 470-477.

733

734